Using Good's Buffers to Control the Anisotropic Structure and Optical Properties of Spiky Gold Nanoparticles for Refractive Index Sensing

Roger M. Pallares,[†] Terrence Stilson,[†] Priscilla Choo,[†] Jingtian Hu,[‡] and Teri W. Odom[*,†,‡,§]

[†]Department of Chemistry, [‡]Department of Materials Science and Engineering, [§]International Institute for Nanotechnology, Northwestern University, Evanston, Illinois 60208, United States

Corresponding Author: *E-mail: todom@northwestern.edu.

ABSTRACT

Spiky gold nanoparticles show structure-tunable optical properties. Most synthetic procedures, however, cannot independently manipulate the overall particle shape, core size, and spike features. Furthermore, conventional protocols rely on cytotoxic and/or strongly bound surfactants that limit applications. This paper reports a set of parameters to manipulate the anisotropic features of spiky gold nanoparticles grown using different biocompatible Good's buffers through a seed-mediated synthesis. Spike dimensions were preserved even when large seeds (up to 100 nm) were used. Finally, we obtained particles with high sensitivity to changes in the refractive index of the surroundings by tuning the spike length and width.

Key Words: Spiky gold nanoparticles; gold nanostars; anisotropic gold nanoparticles; nanoparticle synthesis; Good's buffers; refractive index sensitivity

INTRODUCTION

Size, shape, and dielectric environment determine the physical and chemical properties of anisotropic gold nanoparticles (AuNPs).[1] Among the different morphologies, AuNPs constructed from spherical cores and protruding spikes—spiky nanoparticles—are of interest because they show (1) localized surface plasmon (LSP) resonances tunable by spike and core dimensions;[2] (2) strong electric field enhancements at the tips of spikes that result in the highest surface-enhanced Raman spectroscopy enhancement factors among all particle shapes;[3,4] and (3) sensitive optical responses for local refractive index sensing.[5,6] Spiky AuNPs are typically synthesized through seed-mediated methods, where small seeds (<30 nm) are added to a growth solution containing shape-directing agents.[7,8] These syntheses, however, cannot independently manipulate anisotropic features and size, such as changing spike dimensions without altering the overall particle size. In addition, the strongly bound and usually cytotoxic surfactants used to promote anisotropic growth[9,10] limit the use of spiky AuNPs in biological applications, such as drug delivery[11,12] and imaging.[13]

Biocompatible Good's buffers, such as EPPS, HEPES and MOPS, can be used as both reducing and shape-directing agents of gold salts in the seedless synthesis of gold nanostars (AuNS).[14] Although AuNS seem to lack a well-defined core, they show optical responses similar to spiky AuNPs because of their protruding features.[7,14] AuNS have advantages over spherical particles, such as (1) multiple surface curvatures (positive, negative, neutral) that enhance the relaxivity of particle-bound magnetic resonance imaging contrast agents,[15] (2) higher catalytic performance,[16] and (3) higher emission intensities when used as cavities in random lasing.[17] Because of the room-temperature growth conditions, as-prepared AuNS are highly heterogeneous, and tedious sorting steps are needed to refine the structural distributions.[18,19] A protocol that combines the spiky

features produced by Good's buffers and the monodispersity of seed-mediated growth would represent an advance in the synthesis of anisotropic NPs. An initial attempt to combine HEPES and Au seeds, however, could not produce spiky AuNPs without the addition of a mutagenic reducing agent.[20]

Here we report a seed-mediated synthesis of spiky AuNPs from non-cytotoxic Good's buffers and large (> 30 nm) colloidal Au seeds. The type of buffer (EPPS, HEPES, MOPS) controlled the final AuNP morphology, including particle shape and size and optical properties. Spike and core dimensions were tuned by changing seed concentration and pH. Our protocol allowed to preserve the spike dimensions, which kept the primary LSP wavelength position constant, as the seed size increased from 30 nm to 100 nm. Finally, we found that AuNPs with higher aspect-ratio spikes showed extremely high refractive index sensitivities ($\Delta\lambda/\Delta n$ = 533 nm/RIU) to different bulk solutions.

RESULTS AND DISCUSSION

Seed-mediated growth of spiky AuNPs with Good's buffers

Scheme 1 depicts the synthesis of spiky AuNPs using seeds and Good's Buffers. We first focused on the EPPS buffer because of its recent use in growing anisotropic NPs.[21,22] $HAuCl_4$ (0.2 mM) and EPPS buffer (100 mM, pH 7.0) concentrations were kept constant in all growth solutions

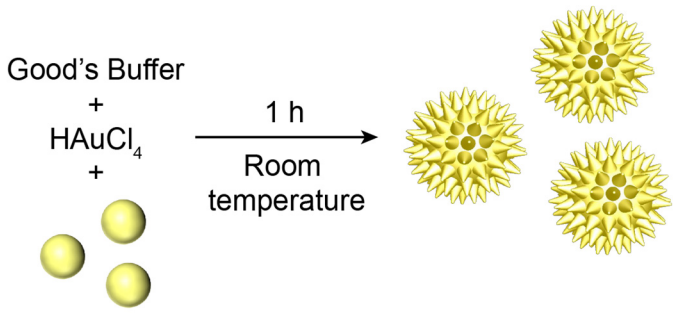

Scheme 1. Seed-mediated growth of spiky AuNPs with Good's buffers

since these conditions produced stable particles in previous seedless protocols.[14,22] The main LSP resonance blue-shifted from 750 to 640 nm as the concentration of 60-nm Au seeds increased (**Figure 1a**), and AuNPs with larger spikes (up to 21 ± 6 nm) and bigger cores (up to 86 ± 5 nm) were obtained from a lower number of seeds (**Figures 1b-c**). Fewer nucleation seeds resulted in higher amounts of Au^{3+} reduced to Au on each seed and the growth of larger particles.

We tested two other Good's buffers with chemical structures similar to EPPS: (1) HEPES, which has the same primary functional group (piperazine ring) and (2) MOPS, which has the same side chain (propane sulfonate) (Figure S1). For particles grown with HEPES buffer (pH 7.0), the addition of higher concentration of 60-nm seeds shifted the LSP from 725 to 750 nm (**Figure 2a**). The spike dimensions were similar for all samples, and the core size decreased with higher seed concentration (Figure S2a). At very low seed concentrations (5 pM), there were some particles that grew through the seedless mechanism (AuNS shape without a spherical core) because of the lack

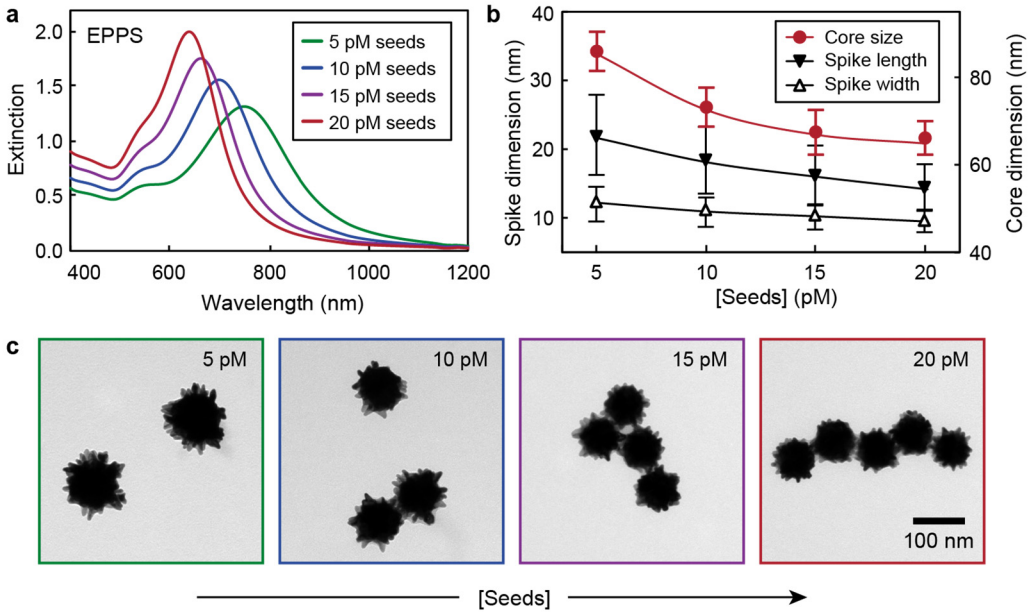

Figure 1. Spiky AuNPs grown with EPPS buffer at pH 7.0 and 60-nm seeds. (**a**) UV-Vis spectra, (**b**) dimensions and (**c**) TEM images of AuNPs grown with EPPS as function of seed concentration.

of nucleation sites. The morphologies of spiky AuNPs obtained using HEPES were similar to the ones synthetized with EPPS because both Good's buffers show comparable radical generation profiles associated with anisotropic NP growth under these experimental concentrations.[22]

MOPS buffer (pH 7.0) with 60-nm Au seeds resulted in both larger and shorter spikes within the same particle (**Figure 2b** and Figure S3). Two LSP bands (at wavelengths λ_1 and λ_2) were observed as result of the different branch lengths (Figure S2b). At low seed concentrations, the particles had higher numbers of long spikes, and the LSP at λ_2 showed higher intensity than λ_1. As the amount of seeds increased and Au^{3+} and MOPS concentrations were kept constant, shorter branches were dominant in the final structures because the available Au was distributed among more seeds. The decrease of spike length resulted in a blue-shift in wavelength of the LSP bands and an increase of the LSP intensity at λ_1. The weak LSP resonance of the core around 550 nm was only visible for particles grown with 5 pM seeds because the LSP of the shorter spikes and core overlapped at high seed concentrations. The LSP position and intensity of the core were

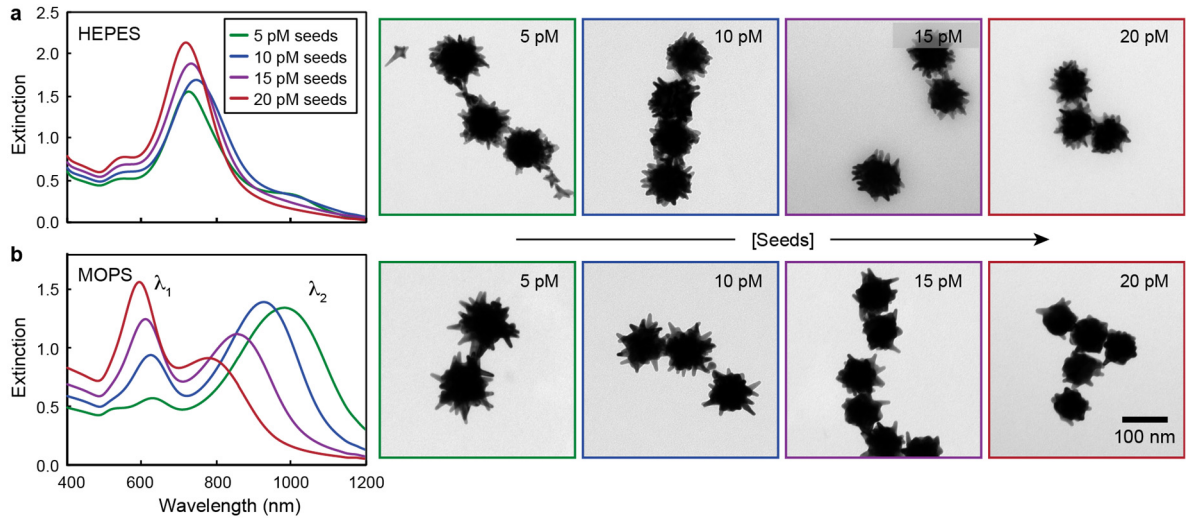

Figure 2. Spiky AuNPs grown with different HEPES and MOPS at pH 7.0 and 60-nm seeds. UV-Vis spectra and TEM images of AuNPs grown with (**a**) HEPES and (**b**) MOPS as function of seed concentration.

similar with previous simulations.[2,7] Since MOPS has only one Au^{3+}-reducing tertiary amine (EPPS and HEPES have two),[14] the reaction kinetics were slower (Figure S4) and produced AuNPs with higher aspect-ratio features compared to EPPS and HEPES. Although spiky AuNPs grown in EPPS, HEPES, and MOPS at pH 7.0 (10-pM seeds) had different spike dimensions, they had similar Feret diameters (Table S1). Lastly, this NP seed-mediated protocol produced between 90 to 100% spiky AuNPs with MOPS (Figure S5) compared to 53% of particles with spikes grown by the seedless method[14] (Figure S6).

Effect of pH on anisotropic particle growth

Next, we studied the seed-mediated growth of spiky AuNPs at different pH (6.0, 6.5 and 7.0) since pH has been identified as a key factor to achieve NPs with anisotropic features.[23] We kept the pH of all solutions below the lowest pK_a of the buffers (MOPS, 7.2) since particles synthesized

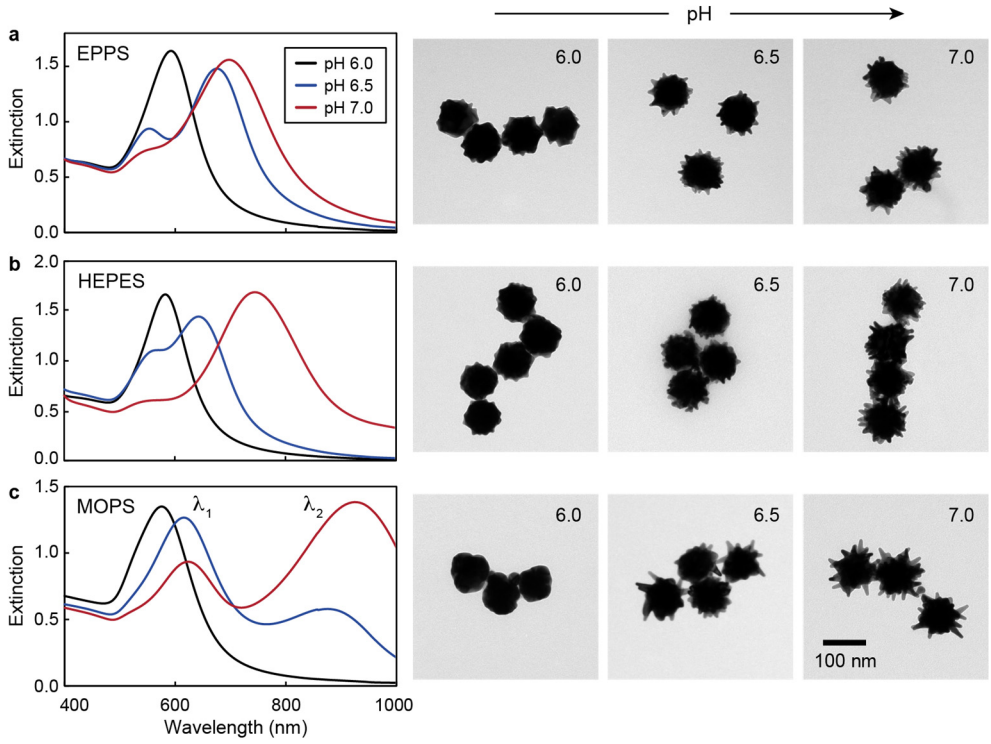

Figure 3. Higher pH promotes the growth of larger spikes. UV-Vis spectra and TEM images of AuNPs grown with 60-nm seeds (10 pM) and (**a**) EPPS, (**b**) HEPES and (**c**) MOPS as function of pH.

in pH above the pK_a are not stable.[14] The lowest pH was 6.0 because HEPES does not grow AuNPs when the pH is below about 5.5.[24] As pH increased, EPPS and HEPES showed similar trends with the LSP wavelength red-shifting from ca. 590 to 700 nm as the spikes became longer (**Figures 3a-b**). For MOPS at pH 6.0, one LSP was recorded ca. 580 nm because the AuNPs had very short branches (**Figure 3c**). Two LSP resonances (at wavelengths λ_1 and λ_2) appeared at pH 6.5 from the growth of spikes with two different lengths within the same particle. At pH 7.0, the resonance at λ_2 further red-shifted and showed higher intensity than λ_1 because there were more particles with higher aspect-ratio branches. These results agree with a previous AuNS study that found that higher aspect-ratio features formed at higher pH[14] because the binding affinity of HEPES for Au increases as the amines from the piperazine ring are deprotonated.[25]

Effect of AuNP size on optical properties

Deconstructing effects of spikes and core on the optical response is difficult because common synthetic protocols change spike features when the particle core size is increased.[26] We addressed this issue by growing AuNPs with distinct core sizes but similar spike dimensions with EPPS

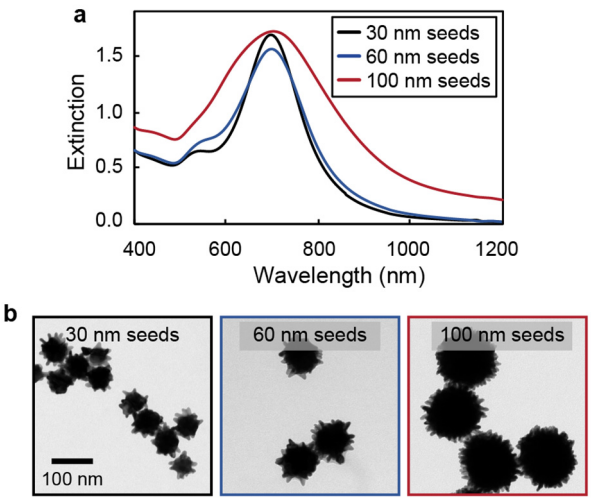

Figure 4. AuNPs with same spike dimensions grow on different seed sizes. (**a**) UV-Vis spectra and (**b**) TEM images of AuNPs grown with EPPS and 30, 60 and 100 nm seeds.

buffer (pH 7.0) and 30, 60 and 100-nm seeds (**Figure 4**). The synthetic conditions were optimized to preserve the spike dimensions (Table S2) from different seeds (Figure S7). Because the spikes were similar for all three particles, the dominant LSP was at ca. 700 nm. An increase in overall AuNP size, however, resulted in broader spectra. The absorbance and scattering portions of the LSP resonances were experimentally measured with absorption dominating at smaller sizes (30 and 60-nm seeds) and the scattering component increasing with core size because of larger particle cross-sections (Figure S8). These trends were consistent with finite-difference time-domain (FDTD) simulations of the spiky AuNPs (Figure S9).

Shape and size effects on refractive index sensitivity

Spiky AuNPs grown in EPPS, HEPES or MOPS at pH 7.0 with similar Feret diameters (96 ± 4, 94 ± 5, and 96 ± 6 nm, respectively) were compared to determine the effect of shape on refractive index (*n*) sensitivity. Different volumes of H_2O and glycerol were combined to change the *n* of the solution (Table S3). When *n* was increased from 1.33 to 1.47, the LSP of all spiky AuNPs red-shifted and broadened (**Figure 5**), which was consistent with previous simulations for spherical and rod-shaped AuNPs.[27] Refractive index sensitivity can be defined as the shift of the LSP resonance after increasing *n* of the medium ($\Delta\lambda/\Delta n$).[28,29] Particles grown with EPPS and HEPES that were similar in shape and size showed comparable sensitivity with $\Delta\lambda/\Delta n$ = 327 and 363 nm/(refractive index unit, RIU), respectively (Figures 5a-b). The LSP at λ_2 of spiky AuNPs grown with MOPS (Figures 5c-d) was the most sensitive to changes in the environment ($\Delta\lambda/\Delta n$ = 533 nm/RIU) because the resonance originated from spikes with longer aspect ratios. The LSP resonance at λ_1, which resulted from shorter aspect ratio spikes and was at bluer wavelengths, was the least sensitive ($\Delta\lambda/\Delta n$ = 210 nm/RIU). These results agree with previous work that found elliptical AuNPs with higher-aspect ratios were more sensitive to changes in the particle

surroundings because of enhanced AuNP polarizability and higher surface area to volume ratio.[30] Finally, we compared spiky AuNPs grown with EPPS (pH 7.0) and 30, 60 and 100-nm seeds to investigate the effect of NP core size on refractive index sensitivity (Figure S10). Although sensitivity increased from 304 to 387 nm/RIU with core size, particle shape had a larger effect than size. These results are consistent with studies on other anisotropic NPs, such as Au nanorods and nanoellipses.[30,31]

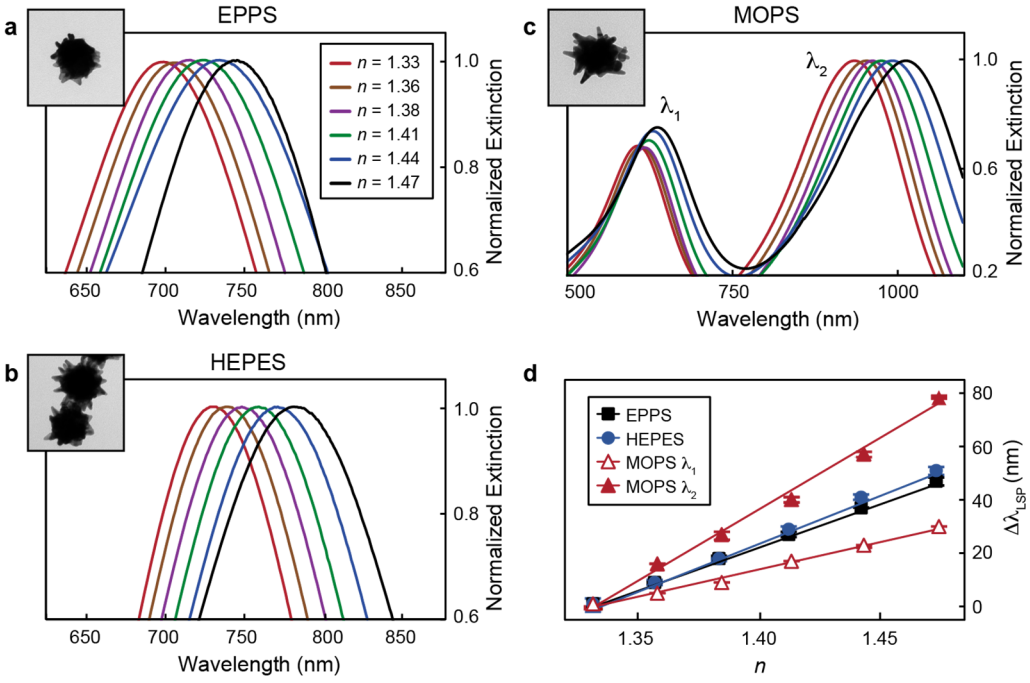

Figure 5. AuNPs with sharper features show higher refractive index sensitivity. TEM and UV-Vis spectra of spiky AuNPs grown with 60-nm seeds (10 pM) and (**a**) EPPS, (**b**) HEPES and (**c**) MOPS in different refractive index environments. The TEM box dimensions are 200 nm × 200 nm. All spectra were normalized by adjusting and scaling the LSP maxima to extinction value of 1.0. For particles grown with MOPS, the normalization was done relative to the more intense LSP resonance (λ_2) (**d**) Shift of the LSP band of different particles as function of refractive index.

CONCLUSIONS

In summary, we established a set of parameters to manipulate the size, shape, and optical properties of spiky AuNPs. This protocol uses biocompatible Good's buffers to promote the

growth of anisotropic features on colloidal cores instead of conventional cytotoxic directing agents and enables individual manipulation of specific features. Spike dimensions and LSP band position were preserved when changing the seed size from 30 up to 100 nm. The high aspect-ratio features of spiky AuNPs grown with MOPS buffer showed the highest bulk refractive index sensitivity. Our procedure expands the library of AuNPs with sharp anisotropic features, which may provide opportunities in biosensing, catalysis, and therapeutic applications.

EXPERIMENTAL SECTION

Materials

4-(2-hydroxyethyl)-1-piperazinepropanesulfonic acid (EPPS), 4-(2-hydroxyethyl)piperazine-1-ethanesulfonic acid (HEPES), 3-(N-morpholino)propanesulfonic acid (MOPS), chloroauric acid, tri-sodium citrate dihydrate (sodium citrate), hydrochloric acid (37%), and nitric acid (70%) were bought from Sigma Aldrich, St. Louis, MO. 30, 60 and 100-nm AuNPs stabilized with citrate and dispersed in water were purchased from Ted Pella Inc., Redding, CA.

Synthesis of spiky AuNPs with Good's buffers and characterization

Spiky AuNPs were synthesized in 20 mL scintillation glass vials (Cole-Parmer, Vernon Hills, IL) by adding 100 mM (final concentration) Good's buffer to AuNP seed solutions of varying concentrations. Each solution was stirred at 400 rpm for 30 s before the addition of 0.2 mM chloroauric acid (final concentration). The resulting solutions were stirred for 30 min and left undisturbed at room temperature for 12 h. The final volume of the solutions was 10 mL.

The extinction spectra of spiky AuNPs were recorded with a Cary 5000 UV-vis-NIR spectrophotometer from Agilent Technologies, Santa Clara, CA. The absorbance spectra were recorded with a Diffuse Reflectance Accessory and a Cary 5000 UV-vis-NIR spectrophotometer, and scattering spectra were calculated by subtracting the absorbance spectra to the extinction ones. AuNP morphologies were characterized with the images obtained by a JEOL 1230 transmission electron microscope, JEOL Ltd, Tokyo, Japan. The spiky AuNP sizes were reported as the average of their Feret diameters (size of the particle in a specific direction). The concentrations of AuNP seeds were quantified by inductively coupled plasma mass spectrometry (ICP-MS, iCAP Q, Thermo Fisher Scientific, Waltham, MA). The AuNP samples were digested before ICP-MS

quantification in a 1:1 mixture of nitric acid and hydrochloric acid for 30 min, and subsequent 20-fold dilution in milli-Q water.

Simulations and data analysis

A script implemented by R programming using the mclust package was used to analyze the size distribution of the nanoparticles and spikes. Bayesian information criterion (BIC) analysis was performed under the assumption that the variance varied between distributions for a range of clusters (number of distributions). Because modeling by two clusters resulted in the lowest BIC value for the spiky AuNPs grown with MOPS, we confirmed the data was made of two different spike populations. The function 'mclustModel' was used to model the distributions, and the averages and standard variations were calculated.

Finite-difference time-domain (FDTD) simulations based on commercial software (FDTD Solution, Lumerical Inc., Vancouver, Canada) were used to model the linear properties (far-field) of spiky AuNPs. The optical constants of Au were taken from Johnson and Christy (400-1200 nm).[32] A uniform mesh size of 0.4 nm was imposed on the particles. The spiky AuNP was placed in a cubic total-field/scattered-field source with a size of 300 nm to calculate the optical cross-sections. A cubic shape analysis group consisting of six frequency-domain monitors with size of 180 nm (350) was placed around the particle to calculate the absorption (scattering) cross-section.

ASSOCIATED CONTENT

Supporting Information. This material is available free of charge via the Internet at http://pubs.acs.org.

Molecular structures of EPPS, HEPES and MOPS, dimensions of spiky AuNPs grown with HEPES and MOPS, reaction kinetics of spiky AuNPs, percent of spiky AuNPs in solution, characterization of spiky AuNPs grown with different seed sizes, comparison between spiky

AuNPs grown by seedless and seed-mediated methods, TEM images of seeds, absorbance and scattering components of particles grown with different seed sizes, refractive index of different water-glycerol solutions, refractive index sensitivities of spiky AuNPs with different core sizes. The authors declare no competing financial interest.

AUTHOR INFORMATION

Corresponding Author. *E-mail: todom@northwestern.edu.

ORCID

Roger M. Pallares: 0000-0001-7423-8706

Priscilla Choo: 0000-0003-1546-2390

Jingtian Hu: 0000-0002-0528-6250

Teri W. Odom: 0000-0002-8490-292X

ACKNOWLEDGMENTS

This work was supported by the National Cancer Institute of the National Institutes of Health under Award Number U54CA199091 (R.M.P., T.W.O.) and the National Science Foundation under CHE-1808502 (P.C.). The content is solely the responsibility of the authors and does not necessarily represent the official views of the National Institutes of Health. T.S. acknowledges the Chemistry of Life Processes Institute for his Lambert Fellowship. Quantification of gold was conducted at the Northwestern University Quantitative Bio-elemental Imaging Center generously supported by NASA Ames Research Center NNA06CB93G.

REFERENCES

(1) Murphy, C. J.; Sau, T. K.; Gole, A. M.; Orendorff, C. J.; Gao, J.; Gou, L.; Hunyadi, S. E.; Li, T. Anisotropic Metal Nanoparticles: Synthesis, Assembly, and Optical Applications. *J. Phys. Chem. B* **2005,** *109* (29), 13857-13870.
(2) Hsiangkuo, Y.; Christopher, G. K.; Hanjun, H.; Christy, M. W.; Gerald, A. G.; Tuan, V.-D. Gold nanostars: surfactant-free synthesis, 3D modelling, and two-photon photoluminescence imaging. *Nanotechnology* **2012,** *23* (7), 75102-75102.
(3) Hastings, S. P.; Swanglap, P.; Qian, Z.; Fang, Y.; Park, S.-J.; Link, S.; Engheta, N.; Fakhraai, Z. Quadrupole-Enhanced Raman Scattering. *ACS Nano* **2014,** *8* (9), 9025-9034.
(4) Solís, D. M.; Taboada, J. M.; Obelleiro, F.; Liz-Marzán, L. M.; García de Abajo, F. J. Optimization of Nanoparticle-Based SERS Substrates through Large-Scale Realistic Simulations. *ACS Photonics* **2017,** *4* (2), 329-337.
(5) Webb, J. A.; Erwin, W. R.; Zarick, H. F.; Aufrecht, J.; Manning, H. W.; Lang, M. J.; Pint, C. L.; Bardhan, R. Geometry-Dependent Plasmonic Tunability and Photothermal Characteristics of Multibranched Gold Nanoantennas. *J. Phys. Chem. C* **2014,** *118* (7), 3696-3707.
(6) Dondapati, S. K.; Sau, T. K.; Hrelescu, C.; Klar, T. A.; Stefani, F. D.; Feldmann, J. Label-free Biosensing Based on Single Gold Nanostars as Plasmonic Transducers. *ACS Nano* **2010,** *4* (11), 6318-6322.
(7) Senthil Kumar, P.; Pastoriza-Santos, I.; Rodríguez-González, B.; Javier García de Abajo, F.; Liz-Marzán, L. M. High-yield synthesis and optical response of gold nanostars. *Nanotechnology* **2007,** *19* (1), 015606-015606.
(8) Nehl, C. L.; Liao, H.; Hafner, J. H. Optical properties of star-shaped gold nanoparticles. *Nano Lett.* **2006,** *6* (4), 683-688.
(9) Koczkur, K. M.; Mourdikoudis, S.; Polavarapu, L.; Skrabalak, S. E. Polyvinylpyrrolidone (PVP) in nanoparticle synthesis. *Dalton Trans.* **2015,** *44* (41), 17883-17905.
(10) Takahashi, H.; Niidome, Y.; Niidome, T.; Kaneko, K.; Kawasaki, H.; Yamada, S. Modification of Gold Nanorods Using Phosphatidylcholine to Reduce Cytotoxicity. *Langmuir* **2006,** *22* (1), 2-5.
(11) Yue, J.; Pallares, R. M.; Cole, L. E.; Coughlin, E. E.; Mirkin, C. A.; Lee, A.; Odom, T. W. Smaller CpG-Conjugated Gold Nanoconstructs Achieve Higher Targeting Specificity of Immune Activation. *ACS Appl. Mater. Interfaces* **2018,** *10* (26), 21920-21926.
(12) Pallares, R. M.; Choo, P.; Cole, L. E.; Mirkin, C. A.; Lee, A.; Odom, T. W. Manipulating Immune Activation of Macrophages by Tuning the Oligonucleotide Composition of Gold Nanoparticles. *Bioconjugate Chem.* **2019**, 10.1021/acs.bioconjchem.9b00316.
(13) Sun, I.-C.; Na, J. H.; Jeong, S. Y.; Kim, D.-E.; Kwon, I. C.; Choi, K.; Ahn, C.-H.; Kim, K. Biocompatible Glycol Chitosan-Coated Gold Nanoparticles for Tumor-Targeting CT Imaging. *Pharm. Res.* **2014,** *31* (6), 1418-1425.
(14) Chandra, K.; Culver, K. S. B.; Werner, S. E.; Lee, R. C.; Odom, T. W. Manipulating the Anisotropic Structure of Gold Nanostars using Good's Buffers. *Chem. Mater.* **2016,** *28* (18), 6763-6769.
(15) Rotz, M. W.; Culver, K. S. B.; Parigi, G.; MacRenaris, K. W.; Luchinat, C.; Odom, T. W.; Meade, T. J. High Relaxivity Gd(III)–DNA Gold Nanostars: Investigation of Shape Effects on Proton Relaxation. *ACS Nano* **2015,** *9* (3), 3385-3396.
(16) Ma, T.; Yang, W.; Liu, S.; Zhang, H.; Liang, F. A Comparison Reduction of 4-Nitrophenol by Gold Nanospheres and Gold Nanostars. *Catalysts* **2017,** *7* (2), 38-48.

(17) Ziegler, J.; Djiango, M.; Vidal, C.; Hrelescu, C.; Klar, T. A. Gold nanostars for random lasing enhancement. *Opt. Express* **2015,** *23* (12), 15152-15159.
(18) Chandra, K.; Kumar, V.; Werner, S. E.; Odom, T. W. Separation of Stabilized MOPS Gold Nanostars by Density Gradient Centrifugation. *ACS Omega* **2017,** *2* (8), 4878-4884.
(19) Culver, K. S. B.; Shin, Y. J.; Rotz, M. W.; Meade, T. J.; Hersam, M. C.; Odom, T. W. Shape-Dependent Relaxivity of Nanoparticle-Based T1 Magnetic Resonance Imaging Contrast Agents. *J. Phys. Chem. C* **2016,** *120* (38), 22103-22109.
(20) Maiorano, G.; Rizzello, L.; Malvindi, M. A.; Shankar, S. S.; Martiradonna, L.; Falqui, A.; Cingolani, R.; Pompa, P. P. Monodispersed and size-controlled multibranched gold nanoparticles with nanoscale tuning of surface morphology. *Nanoscale* **2011,** *3* (5), 2227-2232.
(21) Lu, G.; Forbes, T. Z.; Haes, A. J. SERS detection of uranyl using functionalized gold nanostars promoted by nanoparticle shape and size. *Analyst* **2016,** *141* (17), 5137-5143.
(22) Chandra, K.; Rugg, B. K.; Ratner, M. A.; Wasielewski, M. R.; Odom, T. W. Detecting and Visualizing Reaction Intermediates of Anisotropic Nanoparticle Growth. *J. Am. Chem. Soc.* **2018,** *140* (9), 3219-3222.
(23) Grzelczak, M.; Pérez-Juste, J.; Mulvaney, P.; Liz-Marzán, L. M. Shape control in gold nanoparticle synthesis. *Chem. Soc. Rev.* **2008,** *37* (9), 1783-1791.
(24) Chen, R.; Wu, J.; Li, H.; Cheng, G.; Lu, Z.; Che, C.-M. Fabrication of gold nanoparticles with different morphologies in HEPES buffer. *Rare Metals* **2010,** *29* (2), 180-186.
(25) Xi, W.; Haes, A. J. Elucidation of HEPES Affinity to and Structure on Gold Nanostars. *J. Am. Chem. Soc.* **2019,** *141* (9), 4034-4042.
(26) Barbosa, S.; Agrawal, A.; Rodríguez-Lorenzo, L.; Pastoriza-Santos, I.; Alvarez-Puebla, R. A.; Kornowski, A.; Weller, H.; Liz-Marzán, L. M. Tuning Size and Sensing Properties in Colloidal Gold Nanostars. *Langmuir* **2010,** *26* (18), 14943-14950.
(27) Peña-Rodríguez, O.; Pal, U.; Rodríguez-Iglesias, V.; Rodríguez-Fernández, L.; Oliver, A. Configuring Au and Ag nanorods for sensing applications. *J. Opt. Soc. Am. B* **2011,** *28* (4), 714-720.
(28) Lee, J.; Hasan, W.; Odom, T. W. Tuning the Thickness and Orientation of Single Au Pyramids for Improved Refractive Index Sensitivities. *J. Phys. Chem. C* **2009,** *113* (6), 2205-2207.
(29) Kita, S.; Nozaki, K.; Baba, T. Refractive index sensing utilizing a cw photonic crystal nanolaser and its array configuration. *Opt. Express* **2008,** *16* (11), 8174-8180.
(30) Shabaninezhad, M.; Ramakrishna, G. Theoretical investigation of size, shape, and aspect ratio effect on the LSPR sensitivity of hollow-gold nanoshells. *J. Chem. Phys.* **2019,** *150* (14), 144116-144125.
(31) Lee, K.-S.; El-Sayed, M. A. Gold and Silver Nanoparticles in Sensing and Imaging: Sensitivity of Plasmon Response to Size, Shape, and Metal Composition. *J. Phys. Chem. B* **2006,** *110* (39), 19220-19225.
(32) Johnson, P. B.; Christy, R. W. Optical Constants of the Noble Metals. *Phys. Rev. B* **1972,** *6* (12), 4370-4379.

TOC